

From Kondo to local singlet state in graphene nanoribbons with magnetic impurities

G. S. Diniz,¹ G. I. Luiz,^{2,3} A. Latgé,² and E. Vernek³

¹*Curso de Física, Universidade Federal de Goiás, Jataí, GO 75801-615, Brazil*

²*Instituto de Física, Universidade Federal Fluminense, Niterói, RJ 24210-340, Brazil*

³*Instituto de Física, Universidade Federal de Uberlândia, Uberlândia, MG 38400-902, Brazil*

(Dated: June 4, 2021)

A detailed analysis of the Kondo effect of a magnetic impurity in a zigzag graphene nanoribbon is addressed. An adatom is coupled to the graphene nanoribbon via a hybridization amplitude Γ_{imp} in a *hollow* or *top* site configuration. In addition, the adatom is also weakly coupled to a metallic STM tip by a hybridization function Γ_{tip} that provides a Kondo screening of its magnetic moment. The entire system is described by an Anderson-like Hamiltonian whose low-temperature physics is accessed by employing the numerical renormalization group approach, which allows us to obtain the thermodynamic properties used to compute the Kondo temperature of the system. We find two screening regimes when the adatom is close to the edge of the zigzag graphene nanoribbon: (1) a weak coupling regime ($\Gamma_{\text{imp}} \ll \Gamma_{\text{tip}}$), in which the edge states produce an enhancement of the Kondo temperature T_K and (2) a strong coupling regime ($\Gamma_{\text{imp}} \gg \Gamma_{\text{tip}}$), in which a local singlet is formed, in detriment to the Kondo screening by the STM tip. These two regimes can be clearly distinguished by the dependence of their characteristic temperature T^* on the coupling between the adatom and the carbon sites of the graphene nanoribbon (V_{imp}). We observe that in the weak coupling regime T^* increases exponentially with V_{imp}^2 . Differently, in the strong coupling regime, T^* increases linearly with V_{imp}^2 .

I. INTRODUCTION

Magnetic impurities embedded in a metallic environment exhibit the paradigmatic many-body phenomena, the so-called Kondo effect (KE).¹ Since its explanation in a seminal work by J. Kondo,² this effect has been studied in a variety of different physical systems in all dimensionalities (tree-, two- and one-dimensional systems).³⁻⁷ The capability of manipulating atoms and molecules on metallic surfaces with the aid of a STM tip has renewed the interest on the KE on reduced dimensions, as we have witnessed in the last twenty years.⁸ In fact, the advent of the STM has paved the way to a variety of possibilities for investigating the KE in a controllable way in many different systems.⁹⁻¹¹ The great number of theoretical and experimental studies has proved that the observable physical signature of the KE depends drastically on the bare local density of states of the host system.

To understand the dependence of the Kondo physics with the density of states of the free electrons surrounding the magnetic impurities, recall that the physical mechanism underlying the KE is the *dynamical screening* of the localized magnetic moments of the impurities by the conduction electrons of the host material. This screening is led by an effective anti-ferromagnetic exchange coupling J between the impurity and the surrounding electrons that allows for spin-flip scattering processes involving energies below $k_B T_K$, where k_B is the Boltzmann constant and T_K is the characteristic Kondo temperature. Since these are spin-flip scattering events occurring at low temperatures, they depend strongly on the low-energy density of states of the electrons nearby the localized magnetic moments. This is why metallic systems with nearly constant density of states around the Fermi level E_F [$\rho(E) = \rho_F$] exhibits a typical Kondo

temperature $T_K \propto \exp(-1/\rho_F J)$, but can deviate drastically from this expression if ρ presents important features for E close to E_F . Within the single impurity Anderson model for spin-1/2 magnetic impurity problems,¹² the important quantity entering the expression for T_K is the ratio $U/\Delta(E_F)$, where $\Delta(E) \propto \rho(E)$ is the effective hybridization function and U is the Coulomb repulsion energy at the impurity site. Again, we see that $\rho(E)$ can greatly affect T_K . This is crucially important to explain why it is observed enhanced T_K in peaked or in vanishing T_K for pseudo-gaped effective hybridization function, as discussed for a double quantum dot structure.¹³

A natural two-dimensional system exhibiting an interesting density of state near the Fermi-level is graphene.¹⁴⁻¹⁷ The Dirac cones of the band structure lead to zero-gap density of states $\rho(E) \propto |E|$ resulting in a rich phase diagram with interesting quantum phase transitions.^{18,19} There are indeed great efforts devoted to the Kondo physics in graphene with an impurity coupled¹⁸⁻²⁷ or a vacancy (defect) in the graphene lattice²⁸⁻³² in the recent years. Surprisingly, much less attention has been paid to the KE on graphene nanoribbons.³³ A graphene nanoribbon (GNR) is formed by breaking the translational symmetry of a graphene sheet in one particular direction. There are two common directions for *cutting* the graphene with well defined edge shapes: zigzag (ZGNR) and armchair (AGNR). ZGNRs are particularly interesting because around $k = \pi$ they exhibit simultaneously dispersive bulk and bound edge states.^{34,35} These bound edge states render a strongly peaked local density of states, as depicted in Fig. 1(c).

Because of the sharp peak in the local density of states, if we place a magnetic impurity near one edge of the ZGNR one can expect an important modification on the Kondo physics of the system. In particular, in view of

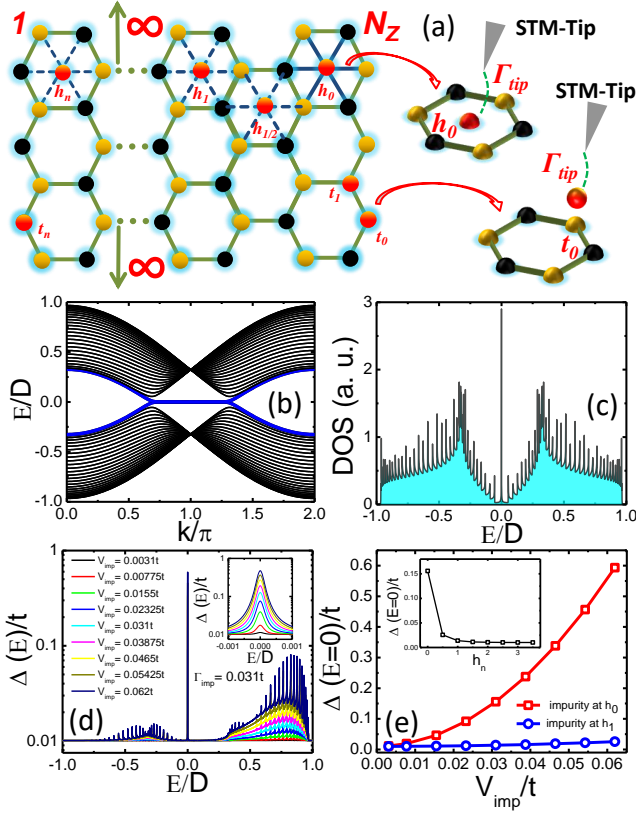


FIG. 1. (a) Schematic representation of N_Z -ZGNR with an impurity located at the hollow site position h_n or at the top site position t_n . The drawing on the right represents a STM tip on the top of the impurity adatom with a coupling strength Γ_{tip} . (b) Electronic structure of a pristine 26-ZGNR highlighting the edge states (blue line). (c) DOS as function of E for the pure graphene. (d) Hybridization function $\Delta(E)$ for different values of impurity coupling strength V_{imp} at h_0 position. Inset: zoom close to $E = 0$ that shows the evolution of the $\Delta(E = 0)$ peak as V_{imp} is enhanced. (e) The $\Delta(E = 0)$ for two different impurity locations h_0 and h_1 as function of V_{imp} . Inset: $\Delta(E = 0)$ vs different adatom position h_n , for $V_{\text{imp}} = 0.031t$.

the discussion above, one can expect this peak to enhance the Kondo temperature of the system. Recent theoretical DFT calculations predict that adatoms are possible generators of localized magnetic moments in graphene and GNR either at hollow and top site positions.^{33,36–42} Motivated by these findings, in this work we are interested in investigating KE of a magnetic impurity placed at two distinct positions in a ZGNR: hollow site and top site.^{43–45} We employ a numerical renormalization group approach (NRG),^{46,47} to address this problem. More precisely, using the NRG approach we calculate the entropy, magnetic susceptibility (from which we can extract the Kondo temperature with the aid of the Wilson's criteria) of the system for an impurity placed at the hollow site for distinct locations along the transversal direction. We find a strong enhancement of the T_K when the impurity

approaches the edge of the ZGNR. More interestingly, in the strong coupling regime between the impurity and the nearby carbon atoms, our calculations suggest that the impurity magnetic moment forms a local singlet state with the edge state of the ZGNR.

This paper is structured as follows: in Sec. II we present the theoretical model describing the hybridization function and the numerical renormalization group approach. In Sec. III the numerical results are discussed. Finally, in Sec. IV we present our conclusions.

II. THEORETICAL MODEL AND METHOD

The system is schematically illustrated in Fig. 1 (a), where a N_Z -ZGNR, with the index N_Z standing to the number of zigzag chains in the transversal direction. To model the single magnetic impurity hosted in the GNR (at the hollow site or at the top site position), we have used the Anderson-like Hamiltonian,¹²

$$H = H_{\text{GNR}} + H_{\text{imp}} + H_{\text{tip}} + H_{\text{GNR-imp}} + H_{\text{imp-tip}}, \quad (1)$$

where the first term describes the GNR that is modeled by a tight-binding Hamiltonian

$$H_{\text{GNR}} = \sum_{i\sigma} (\varepsilon_0 - \mu) c_{i\sigma}^\dagger c_{i\sigma} - t \sum_{\langle i,j \rangle, \sigma} c_{i\sigma}^\dagger c_{j\sigma} \quad (2)$$

in which the operator $c_{i\sigma}^\dagger$ ($c_{i\sigma}$) creates (annihilates) an electron with energy ε_0 and spin σ in the i -th carbon site of the GNR, and μ is the chemical potential that can be externally tuned by a back gate. The matrix element t allows the electron to hop between nearest neighbor carbon sites.¹⁶ The second term in Eq. (1) describes the single level Anderson impurity that is modeled by the interacting Hamiltonian $H_{\text{imp}} = \varepsilon_d n_{d\sigma} + U n_{d\uparrow} n_{d\downarrow}$, where d_σ^\dagger (d_σ) creates (annihilates) an electron with energy ε_d and spin σ at the impurity site, U is the on-site Coulomb interaction and $n_d = n_{d\uparrow} + n_{d\downarrow}$ (with $n_{d\sigma} \equiv d_\sigma^\dagger d_\sigma$) is the total number operator for the impurity electrons. The third term in Eq. (1) describes the STM tip modeled by the Hamiltonian $H_{\text{tip}} = \sum_{\mathbf{k}} \varepsilon_{\mathbf{k}} c_{\mathbf{k}\sigma}^\dagger c_{\mathbf{k}\sigma}$, where $c_{\mathbf{k}\sigma}^\dagger$ ($c_{\mathbf{k}\sigma}$) creates (annihilates) an electron with momentum \mathbf{k} and spin σ in the STM tip. Finally, the last two terms of the Eq. (1) couples the impurity to the GNR and to the STM tip, respectively. They are, respectively, given by

$$H_{\text{GNR-imp}} = \sum_{j,\sigma} V_j c_{j\sigma}^\dagger d_\sigma, \quad (3)$$

and

$$H_{\text{imp-tip}} = \sum_{\mathbf{k}\sigma} (V_{\mathbf{k}} c_{\mathbf{k}\sigma}^\dagger d_\sigma + \text{H.c.}). \quad (4)$$

In Eq. (3) V_j represents the impurity coupling amplitude to the neighboring carbon atoms (later, we set $V_j \equiv V_{\text{imp}}$). For the impurity located at the hollow site position h_n , the sum in j runs over the six carbon atoms

closest to the impurity, while for the top site position t_n , it only corresponds to the single carbon atom which the impurity is coupled to.

A. Hybridization function

The implementation of the NRG to determine the Kondo temperature of the system requires first the determination of the hybridization function, $\Delta(E)$, of the impurity. We do it by using the Green's function method to the non-interacting case ($U = 0$). As the impurity is coupled to both the GNR and to the STM tip, we write $\Delta(E) = \Delta_{\text{tip}}(E) + \Delta_{\text{GNR}}(E)$. To obtain $\Delta_{\text{tip}}(E)$ we model the STM tip by a constant density of state ρ_{tip} and assume a coupling, $V_{\mathbf{k}} = V_{\text{tip}}$ (independent of \mathbf{k}), so that we can write $\Delta_{\text{tip}}(E) = \pi V_{\text{tip}}^2 \rho_{\text{tip}} \equiv \Gamma_{\text{tip}}$. To obtain $\Delta_{\text{GNR}}(E)$ we have implemented the standard surface Green's function approach.^{48,49} The GNR is then divided into three regions: left lead, central region (where the impurity adatom is located) and right lead. The retarded Green's function matrix of the central region is $G_C(E) = (E + i\eta - H_C - \Sigma_L - \Sigma_R)^{-1}$ (omitting the spin indices), with E being the energy of the injected electron (the Fermi energy at a given doping) and $\eta \rightarrow 0$. Here, H_C represents the Hamiltonian describing the central region and $\Sigma_{L/R}$ are the self-energies that describe the influence of the left/right leads. Explicitly, $\Sigma_l = H_{lC}^\dagger g_l H_{lC}$, where g_l is the Green's function for the $l = L, R$ semi-infinite lead obtained through an iterative procedure of the tight-binding Hamiltonian,⁴⁸ and H_{lC} couples each lead to the central region. With the Green's function, we can obtain the self energy of the impurity site $\Delta_{\text{GNR}}(E) = \text{Im}[G_C^{-1}(E)]_{NN}$, where N represents the impurity site inside the central region.

Differently from the graphene case, in which for the impurity located at the top site $\Delta(E)$ is a linear function of $|E|$ (or as $|E|^3$ for the hollow site),^{19,50} in the ZGNR $\Delta(E)$ displays a much more complex dependence on E . In the zigzag GNR, for instance, the presence of the edge state dramatically alters the hybridization function $\Delta(E)$. To illustrate this, in Fig. 1(b) we show the electronic structure of a 26-ZGNR (where the 26 stands for the number of zigzag chains along the transverse direction). The blue curve corresponds to the edge states. Note that it exhibits a flat zero energy plateau around $k = \pi$. This plateau gives rise to a sharp zero-energy peak in the DOS of the pristine 26-ZGNR (in the absence of the impurity), $\rho_{\text{GNR}}^{(0)}(E) = \text{Im Tr}[G_c^{(0)}(E)]$, as shown in Fig. 1(c).

Since the sharp contribution to $\rho_{\text{GNR}}^{(0)}(E)$ is located at the edges of the ZGNR, for the impurity coupled to the carbon atoms close to the edges a strong enhanced hybridization is observed at $E = 0$, as shown in Fig. 1(d). Also, we can notice that several satellite peaks appear, as a consequence of the van Hove singularities in the DOS of the ZGNR.^{34,35} Interestingly, note that while $\rho_{\text{GNR}}^{(0)}(E)$

[Fig. 1(c)] is particle-hole symmetric $\Delta(E)$ [Fig. 1(d)] is not. This is because while the former is calculated in the absence of the impurity, the last is defined with the impurity coupled to the GNR, which for the hollow site breaks particle-hole symmetry of the system, a known behavior for non-bipartite lattices.^{51,52} By increasing the impurity coupling V_{imp} , the zero-energy peak of $\Delta(E = 0)$ also increases. This is better appreciated in the inset of Fig. 1(d). In Fig. 1(e) we show $\Delta(E)$ vs V_{imp} for the impurity placed at h_0 (red squares) and h_1 (blue circles). We first note that $\Delta(E = 0)$ is much larger for the impurity at the position h_0 than in position h_1 , see inset of Fig. 1(e), for $V_{\text{imp}} = 0.031t$ ⁵³, which is consistent with the expected decay of the edge state wave function across the ribbon width. Moreover, we can observe that $\Delta(0) \propto V_{\text{imp}}^2$, similar to the case of an impurity coupled to a metallic surface.¹²

For completeness, we have also analysed a metallic armchair graphene nanoribbon (AGNR) with an adatom at the hollow site, with a similar width as the 26-ZGNR. For this purpose, we choose the 47-AGNR, which means 47 N_A (dimers line) along the transversal direction:³⁴ however we did not find any significant change in the local DOS close to the Fermi level, and consequently for the hybridization function around $E = 0$ for different adatom impurity position along the transversal direction. This is a consequence of the almost flat density of states around $E = 0$ and the absence of edge states for the AGNR.³⁴ For metallic AGNR close to the Fermi level, we expect the Kondo physics to mimic the case of a magnetic impurity hosted in a normal metal, where a nearly constant density of states is expected.

B. Numerical renormalization group approach

To provide the Kondo physics description of the GNR with an impurity adatom, we use the Wilson's numerical renormalization group (NRG) approach.^{46,47} For this purpose, we set the Wilson's discretization parameter as $\Lambda = 2.0$, retaining 2000 many-body states after each iteration, and using the z -averaging in the interval $0.2 \leq z \leq 1.0$, in steps of 0.2.⁵⁴ The entropy is obtained within the canonical ensemble as $S(T) = \beta \langle H \rangle + \ln Z$, where Z correspond to the number of occupied states. Similarly, the magnetic moment is given by $Z^{-1} \sum_n [\langle \Psi_n | S_z^2 | \Psi_n \rangle - \langle \Psi_n | S_z | \Psi_n \rangle] \times e^{-\beta E_n}$. It is important to mention that we seek for the entropy S_{imp} , and magnetic moment χ_{imp} which correspond (approximately) to the contribution of impurity to the entropy and to the magnetic moment, and are defined as the difference of the thermodynamical quantities computed for total Hamiltonian H (with the impurity) and with H_0 (without the impurity). Further technical details can be found, for instance, in Ref. 47 and references therein.

III. NUMERICAL RESULTS

The following results are for the N_Z -ZGNR. To obtain our numerical results, we choose the hopping t such that the half-bandwidth is unity, i.e. $D = 1$, and can be used as our energy unity. With this in mind, we use $U/t = 1$ and the $\Gamma_{\text{tip}} = 0.031t$ for all calculations. This choice, for $V_{\text{imp}} = 0$, the hybridization of the impurity with the STM tip will render a very small Kondo temperature (which depends essentially on the ratio $U/\Gamma_{\text{tip}} \approx 32.3$) that can be estimated by⁵⁵ $k_B T_K \approx \sqrt{\Gamma_{\text{tip}} U} e^{-\pi U/8\Gamma_{\text{tip}}} \approx 5.5 \times 10^{-7}t$ for $\delta = 0$, where $\delta = \varepsilon_d + U/2$. Numerically, T_K is obtained from the magnetic moment, following Wilson's criteria,⁴⁶ $k_B T_K \chi(T_K)/(g\mu_B^2) = 0.0707$, where g is the Langé g -factor and μ_B is the Bohr magneton. With this prescription we find (for $V_{\text{imp}} = 0$) $k_B T_K \approx 9.6 \times 10^{-8}t \equiv k_B T_K^{(0)}$ (this will be used later to rescale our characteristic temperatures).

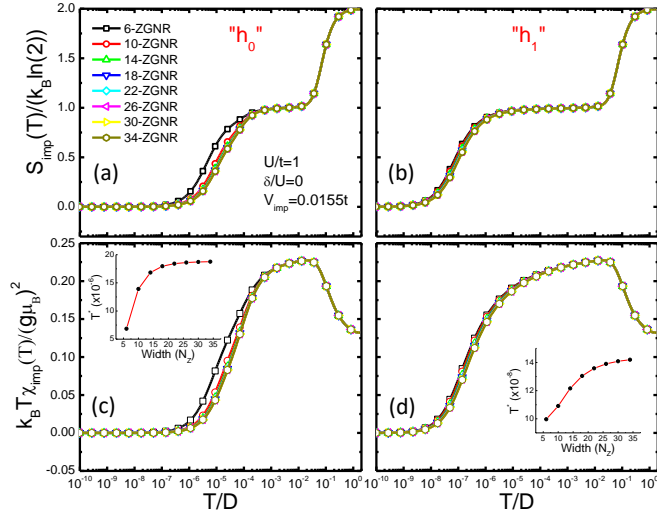


FIG. 2. Entropy (top) and magnetic moment (bottom) vs T for the impurity located at h_0 (left), h_1 (right), and for different widths of the ZGNR. For all panels, $\delta/U = 0$, $U/t = 1$, and $V_{\text{imp}} = 0.0155t$. The insets of panels (c) and (d) show the characteristic Kondo temperature T^* vs N_Z for the corresponding adatom position.

A. Hollow site adatom

To study the effect of the edge state on the Kondo physics screening of the system we first focus on the hollow site position. In Fig. 2 we show the entropy (top) and the magnetic moment (bottom) as function of temperature for different N_Z -ZGNR for $V_{\text{imp}} = 0.0155t$, $\delta/U = 0$, and for the impurity located at h_0 (left) and h_1 (right). Overall, the features observed for the $S_{\text{imp}}(T)$ and $k_B T \chi_{\text{imp}}(T)$ are similar to those known for the traditional single Anderson impurity problem. As shown

in Fig. 2(a) we see two drops of the $S_{\text{imp}}(T)$ as T decreases. The first corresponds to the crossover from the free orbital to the local moment regime while the last one corresponds to the quench of the local magnetic moment by the conduction electrons which characterizes the onset of the KE. Alike, the magnetic moment follows the same feature observed in the single Anderson impurity embedded in a metal. What is interesting here is that, for a given position of the impurity h_0 (left) or h_1 (right), as N_Z increases, S_{imp} and $k_B T \chi_{\text{imp}}$ drop to zero at higher temperatures. This suggests that the *sharpening* of the edge state by increasing N_Z enhances the Kondo temperature of the system. The insets of Figs. 2(c) and 2(d) show the characteristic temperature T^* vs N_Z for the positions h_0 and h_1 , respectively. According to our previous discussion, note that for a given position of the impurity, h_0 or h_1 , T^* with N_Z increases and saturates to a given value. Observe also that consistently with the exponential decay of the wave function as it penetrates across the ZGNR width,³⁴ T^* is much larger for the impurity placed at h_0 [2(c)] than for the situation in which it is placed at h_1 [2(d)]. For the results shown so far we fixed V_{imp} at small value (0.0155t). This assures that even the strongest influence of the edge state of the ZGNR occurring for the position h_0 , it does not change the picture of the Kondo screening.

We address the question whether this picture remains in the regime in which the magnetic impurity is more tightly connected to the ZGNR. To do so, let us turn our attention to the dependence of magnetic moment suppression, as we increase V_{imp} for a given impurity position. Here, we focus on the 26-ZGNR with the adatom at the hollow site position, for which T^* is almost converged [specially for the impurity adatom located at the edge, see the insets of Figs. 2(c) and 2(d)]. Since the drop of $k_B T \chi_{\text{imp}}$ corresponds to a drop in S_{imp} , it suffices to discuss only one of them. Therefore, from now on we will discuss only $k_B T \chi_{\text{imp}}$. In Fig. 3(a) and 3(b) we show the impurity magnetic susceptibility, $k_B T \chi_{\text{imp}}$, vs T for different values of V_{imp} for the impurity placed at h_0 and h_1 , respectively. First, by comparing the curves of Fig. 3(a) with 3(b) we observe that the quenching of the magnetic moments is much more strongly dependent of V_{imp} for h_0 than for h_1 position. Again, this is because the closer is the impurity to the ZGNR edge, the stronger is the hybridization of the impurity orbital with the edge state. This also can be seen in Fig. 3(c) showing $k_B \chi_{\text{imp}}$ vs T for different positions of the impurity on the 26-GNR. Note that the quench of the magnetic moment occurs at much higher temperature for the position h_0 as compared to the other positions. As the impurity is moved far away from the edge, the curves of $k_B T \chi_{\text{imp}}$ rapidly collapse on each other, approaching that one for $V_{\text{imp}} = 0$. This is because far away from the edge the KE is essentially due to the STM tip. Still using Wilson's criteria, from the results of Fig. 3(c) we extract the characteristic temperature T^* below which the magnetic moment is quenched which is shown in Fig. 3(d) vs h_n ,

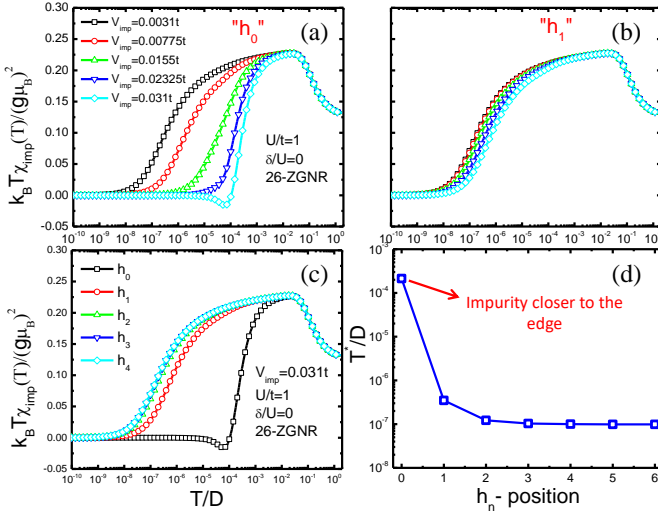


FIG. 3. Magnetic moment vs temperature for the impurity located at h_0 (a) and h_1 (b) and for various values of V_{imp} . (c) Magnetic moment vs temperature for different positions of the adatom h_n with a fixed value of $V_{\text{imp}} = 0.031t$. (d) Kondo temperature, T^* vs position h_n ($n = 0, 1, \dots, 6$), with $V_{\text{imp}} = 0.031t$. [Notice that in this panel we have set the vertical axis in a log scale].

for fixed a $V_{\text{imp}} = 0.031t$. We can observe that T^* drops about three orders of magnitude as the impurity moves from h_0 to h_3 . A remarkable feature observed for large V_{imp} shown in Fig. 3(c), for instance, is that the shape of the magnetic moment for h_0 (black curve) differs significantly from the other ones. The natural question is now: is the suppression of the local magnetic moment for h_0 and large V_{imp} of the Kondo-like type?

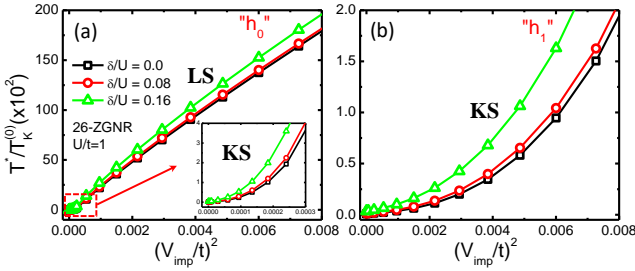


FIG. 4. $T^*/T_K^{(0)}$ as function of $(V_{\text{imp}}/t)^2$ for (a) h_0 and (b) h_1 , for different δ/U ratios. The inset of panel (a) shows a zoom of the region of small values of $(V_{\text{imp}}/t)^2$. The parameters used are in the legend of panel (a) and $T_K^{(0)} = 9.6 \times 10^{-8}t$.

To answer this question, we show in Fig. 4 the $T^*/T_K^{(0)}$ vs V_{imp}^2 , for two different adatom location at the hollow site position h_0 in (a) and h_1 in (b), for different values of δ/U . From Fig. 4(a) we can clearly distinguish two different regimes: for large V_{imp} we note a linear behavior of T^* with V_{imp}^2 but for small V_{imp} the dependence seems

to be exponential. This is better seen in the inset of Fig. 4(a). To understand this, let us remember that when the impurity is coupled to both the tip and the ZGNR, the effective hybridization is given by $\Gamma = \Gamma_{\text{tip}} + \Gamma_{\text{imp}}$. Here, $\Gamma_{\text{imp}} = aV_{\text{imp}}^2$, where a is a constant that depends on the position of the impurity, and the local density of states of the ZGNR. In the small V_{imp} regime we can use the expression for T_K for T^* . Therefore,

$$T^* \sim e^{-\pi U/8\Gamma}. \quad (5)$$

For $\Gamma_{\text{imp}} \ll \Gamma_{\text{tip}}$ we can write

$$\frac{1}{\Gamma} \approx \frac{1}{\Gamma_{\text{tip}}} \left(1 - \frac{\Gamma_{\text{imp}}}{\Gamma_{\text{tip}}} \right). \quad (6)$$

Thus we obtain

$$T^* \sim e^{-\pi U/8\Gamma_{\text{tip}}} e^{(\pi U/8\Gamma_{\text{tip}}^2)\Gamma_{\text{imp}}} \sim T_K^{(0)} e^{bV_{\text{imp}}^2}, \quad (7)$$

where $T_K^{(0)}$ is the Kondo temperature for $V_{\text{imp}} = 0$ and $b = \pi U a / 8\Gamma_{\text{tip}}^2$. Note that the expression (7) is consistent with the exponential behavior of T^* shown in the inset of Fig. 4(a). This shows indeed that in the regime of small V_{imp} the quenching of the magnetic moment is actually of the Kondo type, therefore we call it Kondo singlet (KS) regime and so T^* can be identified as T_K .

In contrast, in the opposite regime, the behavior of T^* can no longer be understood within the picture described above. In this case, the strong coupling between the impurity and the bound edge state (for the position h_0), induces the formation of local singlet (LS). Within this picture, the impurity and the edge state can now be thought as a two hybridized electronic levels with Coulomb repulsion U in one of them. The energy gain to form a LS state in this simple system is known to be $E_S = -4V_{\text{imp}}^2/U$. This explain why in the strong impurity-ZGNR coupling regime $T^* \propto V_{\text{imp}}^2$. In this case, we prefer not to identify T^* as T_K , since here the singlet does not involve the Fermi sea as in the traditional KE. This is actually akin to what was discussed by one of us in Ref. 56. If we now look at Fig. 4(b) this linear behavior of T^* with V_{imp}^2 is not observed (at least for the range of V_{imp} shown). This is because at the position h_1 the influence of the edge state on the impurity remains a small perturbation. Interestingly, as we observe the similar behavior for the different curves of Fig. 5, the two regimes discussed above remain clearly distinguishable for $\delta \neq 0$.

As we have seen above, the behavior of $T^* \sim V_{\text{imp}}^2$ could be nicely understood in terms of the states bound to the edge of the ZGNR. One can argue that if we place the chemical potential close to a van Hove singularity this behavior would no longer be seen. This is because the van Hove singularities are not directly associated to states bound to the edges. To confirm this, we now consider the chemical potential μ at two different van Hove singularities with a relative peak similar to the edge state, and calculate T^* . In Fig. 5(a) we show T^* vs V_{imp}^2 for $\mu = -2.17t$ (black) and $\mu = -2.28t$ (red) and for the two impurity positions h_0 (solid lines) and h_1 (dotted lines).

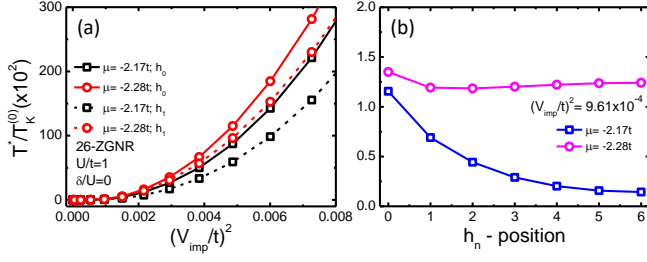


FIG. 5. (a) $T^*/T_K^{(0)}$ vs $(V_{\text{imp}}/t)^2$ for $\mu = -2.17t$ (black) and $-2.28t$ (red) and h_0 (solid) and h_1 (dotted) and. (b) T^* vs adatom position h_n ($n = 0, \dots, 6$), with $(V_{\text{imp}}/t)^2 = 9.61 \times 10^{-4}$. The other parameters are $\delta = 0$, and $U = t$. Here, $T_K^{(0)} = 9.6 \times 10^{-8}t$.

Notice that for all cases T^* increases exponentially with V_{imp}^2 , very similar to the results shown in Fig. 4(b) and in the inset of Fig. 4(a). Confirming our prediction, this shows that in this case, the coupling to the ZGNR no longer favors a LS but leads to KS state with an enhanced T_K . In Fig. 5(b) we show T^* as a function of the impurity position h_n , for the two different chemical potential used in Fig. 5(a). As we see, T^* still decreases quite substantially for $\mu = -2.17t$ [squares (blue)] but for $\mu = -2.28t$ [circle (red)] is almost as the impurity moves far away from the edge. This can be understood based on the electronic states that contribute more to the higher energy van Hove singularities are more extended across the ZGNR.

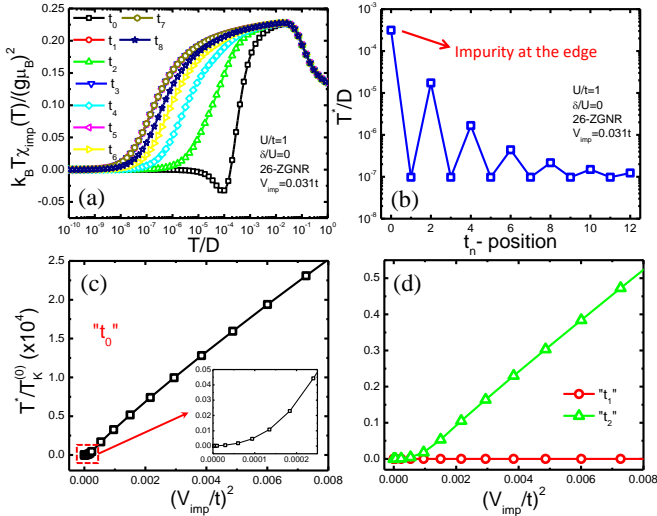


FIG. 6. (a) Magnetic moment vs T for the impurity located at different top site positions t_n . (b) Characteristic temperature, T^* , vs t_n for $V_{\text{imp}} = 0.031t$ [the same as in 3(d)]. (c) and (d) shows T^* vs $(V_{\text{imp}}/t)^2$ for the impurity at the position t_0 , t_1 and t_2 , respectively.

B. Top site adatom

We now investigate if the two screening regimes discussed above also occur for the adatom placed in a top site position. The results obtained in this case are shown in Fig. 6. Fig. 6(a) shows $k_B T_{\text{imp}}$ vs temperature for different positions t_n and for a fixed value of $V_{\text{imp}} = 0.031t$ [as in Fig. 3(c)]. Similar to the hollow site positions, we note that the characteristic temperature T^* (where $k_B T_{\text{imp}}$ drops to zero) increases as the impurity adatom approaches to the edge of the ZGNR. Also, alike the hollow site case, a dramatic change in shape of the $k_B T_{\text{imp}}$ curve occurs for t_0 as compared to the others. This change of regime is accompanied by dramatic drop in T^* as shown in Fig. 6(b), which shows T^* vs t_n . Interestingly, we note that T^* exhibits a damping oscillation as one move the adatom away from the edge of the ZGNR. This behavior was not observed for the hollow site positions. This difference can be understood as follows: in the hollow site case, the adatom is connected to all six carbon atoms of the hexagon, hence the contribution from these neighboring carbons to the corresponding hybridization function is somehow *averaged*. Here, in top site position, the total contribution to the hybridization function comes solely from a single carbon atom. Therefore, a systematic oscillation with an exponential decay of the LDOS across the ZGNR,³⁴ directly influences the hybridization function $\Delta(E)$. In Fig. 6(c) we show T^* vs V_{imp} for position t_0 and in 6(d) we show the same for the positions t_1 and t_2 . We clearly note a linear behavior of T^* for large V_{imp} for both t_0 and t_2 . Also, for the t_0 adatom position (and the subsequent t_{2**n}) we see an exponential behavior of T^* for small V_{imp} . This is better appreciated in the inset of the Fig. 6(c) which shows a zoom of the region of small V_{imp} for the t_0 . For the t_1 position the T^* is practically insensitive to changes in V_{imp} . These results show that the two LS and KS screening regimes indeed occur for both hollow and top site positions, whenever the adatom is placed close to the edge of the ZGNR.

IV. CONCLUSION

We have studied the screening effect of a magnetic impurity (adatom) on a ZGNR. The system was described by an Anderson-like Hamiltonian where the adatom is coupled to the ZGNR as well as to a metallic STM tip. To access the low-temperature physics of the system we have employed a numerical renormalization group approach that allows us to calculate the relevant physical quantities. In particular, we have calculated the magnetic moment of the system, through which we extract the characteristic temperature T^* below which the adatom magnetic moment is screened. We have analyzed either the *hollow* and *top site* adatom configurations. We have found two screening regimes of the adatom magnetic moment: (1) a local singlet (LS), when the adatom

is *strongly* coupled to the bound edge state of the ZGNR and (2) a Kondo singlet (KS) in the *weak* coupling case. The system crosses over the LS to the usual KS either as the impurity is moved away from the edge of the ZGNR or when its coupling V_{imp} to the ZGNR is small. These two screening regimes are well defined by the behavior of the characteristic temperature T^* with V_{imp} . In the LS regime, T^* increases linearly with V_{imp}^2 whereas in the KS it increases exponentially with V_{imp}^2 . We have shown that in the LS regime, the linear dependence of T^* with V_{imp}^2 is consistent with a singlet state formed between the magnetic moment of the impurity, and the one of an electron in the bound edge state. Interestingly, the KS can be understood in terms of an enhancement of the Kondo temperature as V_{imp} increases. In this sense, in the LS regime the ZNGR state that is bound to the edge

competes with the Kondo screening of the adatom magnetic moment by the conduction electrons of the STM tip, whereas in the KS case the ZGNR extended state cooperates with the Kondo screening by the STM tip. Our results are important to the comprehension of the Kondo physics in graphene nanoribbons and, given the relative simplicity of the physical system studied here, we believe that these results can be readily confirmed in STM experiments.

V. ACKNOWLEDGMENTS

We thank R. Žitko for his assistance in the NRG Ljubljana code.⁵⁷ We acknowledge financial support received from CAPES, FAPEMIG, FAPERJ and CNPq.

-
- ¹ A. C. Hewson, *The Kondo problem to heavy fermions* (Cambridge University Press, 1993).
 - ² J. Kondo, *Progress of Theoretical Physics* **32**, 37 (1964).
 - ³ S. Ernst, S. Kirchner, C. Krellner, C. Geibel, G. Zwicknagl, F. Steglich, and S. Wirth, *Nature* **474**, 362 (2011).
 - ⁴ P. Jarillo-Herrero, J. Kong, H. S. van der Zant, C. Dekker, L. P. Kouwenhoven, and S. De Franceschi, *Nature* **434**, 484 (2005).
 - ⁵ J. Nygard, D. H. Cobden, and P. E. Lindelof, *Nature* **408**, 342 (2000).
 - ⁶ S. Sasaki, S. De Franceschi, J. M. Elzerman, W. G. van der Wiel, M. Eto, S. Tarucha, and L. P. Kouwenhoven, *Nature* **405**, 764 (2000).
 - ⁷ D. Goldhaber-Gordon, H. Shtrikman, D. Mahalu, D. Abusch-Magder, U. Meirav, and M. A. Kastner, *Nature* **391**, 156 (1998).
 - ⁸ L. Kouwenhoven and L. Glazman, *Physics World* **14**, 33 (2001).
 - ⁹ H. C. Manoharan, C. P. Lutz, and D. M. Eigler, *Nature* **403**, 512.
 - ¹⁰ G. A. Fiete, G. Zarand, B. I. Halperin, and Y. Oreg, *Phys. Rev. B* **66**, 024431 (2002).
 - ¹¹ V. Iancu, A. Deshpande, and S.-W. Hla, *Phys. Rev. Lett.* **97**, 266603 (2006).
 - ¹² P. W. Anderson, *Phys. Rev.* **124**, 41 (1961).
 - ¹³ L. G. G. V. Dias da Silva, N. P. Sandler, K. Ingersent, and S. E. Ulloa, *Phys. Rev. Lett.* **97**, 096603 (2006).
 - ¹⁴ K. S. Novoselov, A. K. Geim, S. V. Morozov, D. Jiang, Y. Zhang, S. V. Dubonos, I. V. Grigorieva, and A. A. Firsov, *Science* **306**, 666 (2004).
 - ¹⁵ K. S. Novoselov, V. I. Fal'ko, L. Colombo, P. R. Gellert, M. G. Schwab, and K. Kim, *Nature* **490**, 192 (2012).
 - ¹⁶ A. H. Castro Neto, F. Guinea, N. M. R. Peres, K. S. Novoselov, and A. K. Geim, *Rev. Mod. Phys.* **81**, 109 (2009).
 - ¹⁷ A. K. Geim and K. S. Novoselov, *Nat. Mater.* **6**, 183 (2007).
 - ¹⁸ L. Fritz and M. Vojta, *Reports on Progress in Physics* **76**, 032501 (2013).
 - ¹⁹ D. A. Ruiz-Tijerina and L. G. G. V. Dias da Silva, *Phys. Rev. B* **95**, 115408 (2017).
 - ²⁰ L. Li, Y.-Y. Ni, Y. Zhong, T.-F. Fang, and H.-G. Luo, *New Journal of Physics* **15**, 053018 (2013).
 - ²¹ K. Sengupta and G. Baskaran, *Phys. Rev. B* **77**, 045417 (2008).
 - ²² T. O. Wehling, A. V. Balatsky, M. I. Katsnelson, A. I. Lichtenstein, and A. Rosch, *Phys. Rev. B* **81**, 115427 (2010).
 - ²³ S.-P. Chao and V. Aji, *Phys. Rev. B* **83**, 165449 (2011).
 - ²⁴ Z.-G. Zhu and J. Berakdar, *Phys. Rev. B* **84**, 165105 (2011).
 - ²⁵ J. Jobst, F. Kisslinger, and H. B. Weber, *Phys. Rev. B* **88**, 155412 (2013).
 - ²⁶ M. Kharitonov and G. Kotliar, *Phys. Rev. B* **88**, 201103 (2013).
 - ²⁷ D. Mastrogiuseppe, A. Wong, K. Ingersent, S. E. Ulloa, and N. Sandler, *Phys. Rev. B* **90**, 035426 (2014).
 - ²⁸ J.-H. Chen, L. Li, W. G. Cullen, E. D. Williams, and M. S. Fuhrer, *Nat. Phys.* **7**, 535 (2011).
 - ²⁹ P. Haase, S. Fuchs, T. Pruschke, H. Ochoa, and F. Guinea, *Phys. Rev. B* **83**, 241408 (2011).
 - ³⁰ T. Kanao, H. Matsuura, and M. Ogata, *Journal of the Physical Society of Japan* **81**, 063709 (2012).
 - ³¹ A. K. Mitchell and L. Fritz, *Phys. Rev. B* **88**, 075104 (2013).
 - ³² V. G. Miranda, L. G. G. V. Dias da Silva, and C. H. Lewenkopf, *Phys. Rev. B* **90**, 201101 (2014).
 - ³³ D. Krychowski, J. Kaczkowski, and S. Lipinski, *Phys. Rev. B* **89**, 035424 (2014).
 - ³⁴ K. Nakada, M. Fujita, G. Dresselhaus, and M. S. Dresselhaus, *Phys. Rev. B* **54**, 17954 (1996).
 - ³⁵ K. Wakabayashi, Y. Takane, M. Yamamoto, and M. Sigrist, *New Journal of Physics* **11**, 095016 (2009).
 - ³⁶ H. Sevinçli, M. Topsakal, E. Durgun, and S. Ciraci, *Phys. Rev. B* **77**, 195434 (2008).
 - ³⁷ H. Johll, H. C. Kang, and E. S. Tok, *Phys. Rev. B* **79**, 245416 (2009).
 - ³⁸ E. J. G. Santos, A. Ayuela, and D. Snchez-Portal, *New Journal of Physics* **12**, 053012 (2010).
 - ³⁹ M. P. Lima, A. J. R. da Silva, and A. Fazzio, *Phys. Rev. B* **84**, 245411 (2011).
 - ⁴⁰ A. V. Krasheninnikov, P. O. Lehtinen, A. S. Foster, P. Pyykkö, and R. M. Nieminen, *Phys. Rev. Lett.* **102**, 126807 (2009).

- ⁴¹ J. Ding, Z. Qiao, W. Feng, Y. Yao, and Q. Niu, Phys. Rev. B **84**, 195444 (2011).
- ⁴² Y. Mao, J. Yuan, and J. Zhong, Journal of Physics: Condensed Matter **20**, 115209 (2008).
- ⁴³ T. Eelbo, M. Waśniowska, P. Thakur, M. Gyamfi, B. Sachs, T. O. Wehling, S. Forti, U. Starke, C. Tieg, A. I. Lichtenstein, and R. Wiesendanger, Phys. Rev. Lett. **110**, 136804 (2013).
- ⁴⁴ F. Donati, Q. Dubout, G. Autès, F. Patthey, F. Calleja, P. Gambardella, O. V. Yazyev, and H. Brune, Phys. Rev. Lett. **111**, 236801 (2013).
- ⁴⁵ H. González-Herrero, J. M. Gómez-Rodríguez, P. Mallet, M. Moaied, J. J. Palacios, C. Salgado, M. M. Ugeda, J.-Y. Veuillen, F. Yndurain, and I. Brihuega, Science **352**, 437 (2016).
- ⁴⁶ K. G. Wilson, Rev. Mod. Phys. **47**, 773 (1975).
- ⁴⁷ R. Bulla, T. A. Costi, and T. Pruschke, Rev. Mod. Phys. **80**, 395 (2008).
- ⁴⁸ M. B. Nardelli, Phys. Rev. B **60**, 7828 (1999).
- ⁴⁹ M. P. L. Sancho, J. M. L. Sancho, and J. Rubio, Journal of Physics F: Metal Physics **14**, 1205 (1984).
- ⁵⁰ B. Uchoa, T. G. Rappoport, and A. H. Castro Neto, Phys. Rev. Lett. **106**, 016801 (2011).
- ⁵¹ E. Müller-Hartmann, Journal of Low Temperature Physics **99**, 349 (1995).
- ⁵² D. O. Demchenko, A. V. Jura, and J. K. Freericks, Phys. Rev. Lett. **92**, 216401 (2004).
- ⁵³ Here we have also calculated $\Delta(E = 0)$ for the adatom located at intermediate hollow positions $h_{1/2}, h_{3/2}, \dots, h_{7/2}$. Later, we will consider only at h_n , for n integer without loss of generality for the thermodynamical results.
- ⁵⁴ R. Žitko and T. Pruschke, Phys. Rev. B **79**, 085106 (2009).
- ⁵⁵ F. D. M. Haldane, Phys. Rev. Lett. **40**, 416 (1978).
- ⁵⁶ E. Vernek, P. A. Orellana, and S. E. Ulloa, Phys. Rev. B **82**, 165304 (2010).
- ⁵⁷ R. Žitko, NRG Ljubljana - open source NRG code available at <http://nrgljublana.ijs.si>.